Environmental Science Nano

PAPER

View Article Online
View Journal | View Issue

Cite this: *Environ. Sci.: Nano*, 2018, 5, 1694

Release, detection and toxicity of fragments generated during artificial accelerated weathering of CdSe/ZnS and CdSe quantum dot polymer composites†

Miranda J. Gallagher, [a] Joseph T. Buchman, [b] Tian A. Qiu, [b] Bo Zhi, [b] Taeyjuana Y. Lyons, [c] Kaitlin M. Landy, [b] Zeev Rosenzweig, [c] Christy L. Haynes [b] and D. Howard Fairbrother *[a]

Next generation displays and lighting applications are increasingly using inorganic quantum dots (QDs) embedded in polymer matrices to impart bright and tunable emission properties. The toxicity of some heavy metals present in commercial QDs (*e.g.* cadmium) has, however, raised concerns about the potential for QDs embedded in polymer matrices to be released during the manufacture, use, and end-of-life phases of the material. One important potential release scenario that polymer composites can experience in the environment is photochemically induced matrix degradation. This process is not well understood at the molecular level. To study this process, the effect of an artificially accelerated weathering process on QD–polymer nanocomposites has been explored by subjecting CdSe and CdSe/ZnS QDs embedded in poly(methyl methacrylate) (PMMA) to UVC irradiation in aqueous media. Significant matrix degradation of QD–PMMA was observed along with measurable mass loss, yellowing of the nanocomposites, and a loss of QD fluorescence. While ICP-MS identified the release of ions, confocal laser scanning microscopy and dark-field hyperspectral imaging were shown to be effective analytical techniques for revealing that QD-containing polymer fragments were also released into aqueous media due to matrix degradation. Viability experiments, which were conducted with *Shewanella oneidensis* MR-1, showed a statistically significant decrease in bacterial viability when the bacteria were exposed to highly degraded QD-containing polymer fragments. Results from this study highlight the need to quantify not only the extent of nanoparticle release from a polymer nanocomposite but also to determine the form of the released nanoparticles (*e.g.* ions or polymer fragments).

Received 1st March 2018,
Accepted 30th May 2018

DOI: 10.1039/c8en00249e

rsc.li/es-nano

Environmental significance

Elucidating the long term environmental impact of quantum dot (QD)-enabled consumer products depends upon identifying the nature and toxicity of fragments released as a consequence of photochemical weathering. To address this question, a polymer (PMMA) containing Cd-based QDs was exposed to different periods of artificial accelerated weathering. Nanoparticle-containing fragments, released into solution as the polymer matrix degraded, were detected and analyzed with confocal laser scanning microscopy and dark-field hyperspectral imaging. The toxicity of these released fragments towards *Shewanella oneidensis* MR-1 increased as weathering advanced. These findings identify analytical techniques suitable for characterizing QDs in polymer-containing fragments and the role that different forms of released nanomaterials (*e.g.* ions *vs.* QD-containing fragments) have in terms of biological impact.

Introduction

Nanomaterials often have unique physicochemical properties compared to bulk materials that make them attractive for use in consumer products. Currently, the Project on Emerging Nanotechnology by the Woodrow Wilson International Center estimates that over 1800 products contain nanomaterials.[1] The nanomaterials incorporated into polymer-based consumer

[a] *Department of Chemistry, Johns Hopkins University, Baltimore, MD, 21218, USA. E-mail: howardf@jhu.edu*
[b] *Department of Chemistry, University of Minnesota, Minneapolis, MN, 55455, USA*
[c] *Department of Chemistry, University of Maryland Baltimore County, Baltimore, MD, 21250, USA*

† Electronic supplementary information (ESI) available: Photographs of the CdSe/ZnS–PMMA composites in the reaction vessel before and after degradation, library for HSI SAM, QD agglomeration area calculation of CdSe/ZnS–PMMA solid, a table of solution pH, XPS of the starting materials and degraded nanocomposites, solid ATR-FTIR of nanocomposites before and after degradation, time dependent mass loss, PL difference spectra of PMMA from CdSe/ZnS–PMMA, full spectrum wavelength dependent CLSM of CdSe/ZnS–PMMA and PMMA, and HSI of fragments released from photodegradation of PMMA, CdSe–PMMA and CdSe/ZnS–PMMA. See DOI: 10.1039/c8en00249e

products are generally chosen to impart specific functionalities. For instance, polymers are modified by the inclusion of nanodiamond or carbon nanotubes (CNTs) for strength,[2,3] silver nanoparticles for antibiotic properties,[4] and quantum dots (QDs) to impart particular optical properties.[5]

The unique optical properties of QDs are a consequence of the size of the particle being smaller than the Bohr radius of the atom, giving rise to a quantum confinement effect. Accordingly, the emission wavelength of the QDs can be precisely tuned by adjusting the size, shape, and composition of the QD.[6] Popular inorganic QDs which contain II–VI elements such as CdS, CdSe, and CdTe[7] are often capped with a shell (*e.g.* ZnS is used as a cap on CdSe QDs), which increases the emission quantum yield by passivating trap sites at the surface while also providing protection against environmental (*e.g.* photo-oxidative) degradation. CdSe/ZnS core/shell quantum dots display size tunable narrow emission peaks with high emission quantum yield across a broad range of the visible spectrum; as such, they encompass a significant market share of light display technologies.[5] In these applications, CdSe/ZnS quantum dots are embedded into a proprietary conductive polymer matrix that makes up the screen of smart displays, such as the Amazon Kindle Fire 7″ HDX. In other applications, CdSe/ZnS–polymer LEDs, (QLEDs) are used as solid state lighting components, for example, in indoor farming as less heat is produced than from conventional lamps. QLEDs are fabricated by either mixing QDs into the LED structure during processing for electrically induced emission[8] or functionalizing an existing LED substrate for optically induced emission,[9,10] as used here. As an optically transparent polymer with good chemical stability, poly(methyl methacrylate) (PMMA) is an ideal polymer matrix in which to incorporate QDs for lighting purposes.[11] In this study, CdSe and CdSe/ZnS quantum dots were embedded in PMMA to simulate a substrate-functionalized QLED.

When nanomaterials are used to create new products, it is necessary to evaluate their potential adverse impacts on the environment and human health. Cadmium–containing QDs are toxic to cell lines and organisms at various trophic levels.[12–14] The toxic effect is ascribed to the release of Cd^{2+} ions and the generation of reactive oxygen species (ROS). For example, apoptosis of human HL-60 cells was caused by Cd^{2+} ions.[15] In saltwater-dwelling *P. tricornutum* ROS production by CdSe/ZnS is evidenced by the measured increases in superoxide dismutase and catalase expression. Detected with a dichlorofluorescein assay, production of *P. tricornutum* intracellular ROS increased as the concentration of CdSe/ZnS in solution increased.[16] Furthermore, production of ROS superoxide by PEGylated CdSe/ZnS aqueous QDs has been quantitatively measured *ex situ* with electron paramagnetic resonance,[17] while other ROS have been observed when organisms including *D. melanogaster*, human neuroblastomas, and mice livers are exposed to CdSe/ZnS QDs.[18–20] Previous studies have also shown that the presence of a ZnS shell often reduces toxicity, possibly due to a decrease in the photooxidation rate and/or the extent of Cd^{2+} ion dissolution from the core.[14]

Nanoparticles, such as QDs, contained in consumer products, can be released at any stage of product life cycle (*i.e.* during manufacture, use, or end-of-life/disposal). For nanoparticles embedded in polymer composites, four potential mechanisms of release have been identified by T. V. Duncan: i) diffusion, ii) desorption, iii) dissolution, and iv) matrix degradation.[21] The first three are passive forms of release which occur in the absence of polymer degradation. An example of passive release from QD–polymer composites was observed in a study designed to model nanoparticle release characteristics from food packaging.[22] This potential release scenario was examined in an accelerated leaching approach by exposing nanocomposites composed of CdSe/ZnS QDs embedded in low density polyethylene (LDPE) to acidic and oxidative environments at elevated temperatures (75 °C). Results showed the release of ions into the surrounding media occurs by dissolution of embedded QDs, with ZnS shells dissolving first followed by CdSe cores. The extent of ion release was also found to depend on the size of the QDs, with smaller QDs releasing more ions than larger particles over the same timescale and under the same solution conditions.[22] In another passive release case study, a commercial QD-acrylate nanocomposite, QuantumLight™, was degraded by a solvent infiltration mechanism distinct from surface leaching.[9] The CdSe/ZnS-containing QuantumLight™ released no nanoparticles and only ions into solution in quantities that were strongly dependent upon the solution conditions. Results from this study found significant cadmium release only occurred in strong acidic conditions, nitric acid (pH 0.16) and gastric acid (pH 1.12), indicating a general resilience to leaching of the polymer nanocomposite through passive release.[9]

In contrast to passive release, active release from polymer nanocomposites occurs when nanoparticles are released as a result of the polymer matrix itself degrading, during processes such as mechanical abrasion or photodegradation.[21] Motivated by the desire to assess changes in product efficacy and the effective lifetime of the product, polymer degradation studies have tended to focus on the effect of degradation upon the material itself with little effort to collect released materials.[23] The need to better understand the potential hazards posed by nanoparticles in the environment has, however, provided the motivation for several active release studies in the past few years; these studies focused on identifying the nature and extent of nanoparticles and nanoparticle-containing fragments released from nano-enabled products as a consequence of weathering,[24] including TiO_2 from an acrylic urethane coating[25] and CNTs from polymer nanocomposites.[26,27] Active release of QDs from polymer composites has, however, not been previously studied.

In principle, the weathering of a polymer nanocomposite can occur during the use or the end-of-life phase. Although polymer photodegradation can be studied by exposing samples to solar irradiance (*e.g.* at a hot desert test site),[28] natural photodegradation in the environment is typically too slow to be followed experimentally (*e.g.* timescale of years).

Consequently, the most common experimental approach is to use accelerated or artificial weathering conditions. Specific methods and experimental designs vary; for example, polymer samples have been exposed to accelerated weathering using an ASTM G90 Fresnel-reflecting solar concentrator-accelerated weathering machine,[29] an Atlas Xenon Weather-Ometer,[30,31] or the SPHERE at the NIST Accelerated Weathering Laboratory in Gaithersburg, MD.[32] Each method uses an intense light source (*e.g.* concentrated solar, xenon arc lamp, mercury lamp) that contains a broad spectrum of visible and UV light.

In the present study, the artificial accelerated weathering[33] of polymer nanocomposites composed of CdSe and CdSe/ZnSe quantum dots embedded in poly(methyl methacrylate), $(C_5O_2H_8)_n$, has been performed. Previous wavelength-dependent studies have established that PMMA is photodegraded by <320 nm light as a result of polymer chain scission and direct photon absorption by the carbonyl chromophore.[34] Given that the fraction of solar flux reaching the Earth's surface below 320 nm is very small, the natural photochemical weathering of PMMA is extremely low, and accelerated PMMA polymer matrix photodegradation using an intense light source is necessary for laboratory studies.[35] For this reason, we conducted artificial accelerated weathering of PMMA composites with 254 nm UVC light.

Three different QD–polymer nanocomposites were studied: CdSe–PMMA, CdSe/ZnS–PMMA, and quantum dot-free PMMA. Polymer nanocomposites were placed in phosphate-buffered 18 MΩ cm water and photodegraded with UVC light in an open system. The released particles were collected in the water and analyzed over time with inductively coupled plasma mass spectrometry (ICP-MS), confocal laser scanning microscopy (CLSM), and dark-field microscopy. The effect of irradiation on the polymer nanocomposites was also studied over time with an array of analytical techniques, including scanning electron microscopy (SEM), X-ray photoelectron spectroscopy (XPS), attenuated total internal reflection Fourier-transform infrared spectroscopy (ATR-FTIR), and CLSM. A particular point of emphasis in this study has been the detection and environmental impact of polymer fragments containing QDs.

ICP-MS can identify the nature and/or concentration of dissolved ions released into water during polymer matrix degradation, including ions released from QD–polymer composites.[9,21] When combined with centrifugal filtration separation techniques, ICP-MS can also quantify the ratio of released nanoparticles to released ions.[9] Single-particle ICP-MS (spICP-MS) can discriminate and quantify ions and nanoparticles. spICP-MS can, however, only discern the presence of nanoparticles with an element-dependent size limitation of 11–20 nm for cadmium, 21–80 nm for zinc, and >200 nm for selenium.[36,37] These lower limits are, unfortunately, in excess of the 1.32 and 2.26 nm-diameter quantum dots used in this study and in most commercial products.

In addition to ions and discrete nanoparticles, fragments released during the active photodegradation of polymer nanocomposites are also hypothesized here to contain nanoparticles embedded within polymer fragments. The observation, analysis, and quantification of these species is significantly more challenging than for ions or nanoparticles. Thus, spICP-MS detection of nanoparticles within polymer composites has yet to be reported, as extensive separation techniques would be needed. Transmission electron microscopy (TEM) was used to locate released CNTs-polymer fragments[26] in a four-laboratory study by Wohlleben *et al.*, where CNT-polymer composites were irradiated with a xenon-arc lamp for 2000 h (ISO 4892-2). Although TEM has the requisite sensitivity, can directly image and confirm the presence of nanoparticles, as well as resolve composition (individual CNTs *vs.* embedded in polymer fragments), it is a vacuum-based technique which often involves extensive sample preparation and has low sampling efficiency.

This work focused on the use of two microscopy techniques to detect the presence of nanoparticle-containing polymer fragments released into aqueous solution. Specifically, CLSM was used to detect the presence of released photoluminescent quantum dots embedded within polymer fragments. Unfortunately, emission-dependent techniques like CLSM cannot be used to detect transformed nanomaterials, such as QDs, which have lost their nascent photoluminescence after photodegradation. This type of released fragment can be discerned, however, using dark-field microscopy, where nanoparticles are detected based on light scattering. In particular, CytoViva® dark-field hyperspectral imaging (HSI) microscopy has been recently implemented to determine the location of NPs in biological tissues,[38,39] such as silver nanoparticles within *S. oneidensis*.[4] HSI provides a tool for identifying QDs in complex matrices such as biological tissues[38,39] and bacteria[4] without relying on photoluminescence. Here, scattering spectra were collected, spectral libraries were constructed, and pixels containing materials of interest (*i.e.* QDs) were located using the spectral angle mapper (SAM),[40,41] an integrated function within the CytoViva® imaging system.

In addition to identifying the nature of the released PMMA, CdSe–PMMA and CdSe/ZnS–PMMA fragments, a primary toxicity screen was conducted. For these purposes, *Shewanella oneidensis* MR-1 (*S. oneidensis*) was chosen as a model bacterial system because of the ubiquitous presence of genus *Shewanella* in different environments, such as soils, sediments, and marine habitats, making it likely to be exposed to released nanocomposite fragments. *S. oneidensis* has an important environmental role by contributing to geochemical nutrient cycling due to its ability to reduce a wide range of metals.[42] For instance, *S. oneidensis* reduces selenite to Se^0 through its use of anaerobic respiration reductases,[43] but less is known about its ability to interact with the cadmium and zinc present in QDs. Any impact of the fragments generated during the photodegradation of QD nanocomposite on *S. oneidensis* therefore, provides information that could be used to assess the more general impact of QD–PMMA fragments on the environment.

Experimental

Particle synthesis and characterization

CdSe/ZnS core/shell QDs were synthesized using a hot-injection method for core growth, followed by the sequential, layer-by-layer growth of the shell using the successive ionic layer adsorption and reaction (SILAR) synthesis.[44] The synthesis of CdSe/ZnS core/shell QDs was carried out following a well-established protocol.[45] Chemicals were purchased from Sigma Aldrich, Acros Organics, and Fisher Scientific. Briefly, a selenium precursor solution was prepared in a 20 mL scintillation vial, which was then sealed, heated, and sonicated to ensure complete dissolution of the Se. The mixture was then degassed under vacuum and backfilled with nitrogen gas. A Cd precursor solution was prepared, added to a 50 mL three-necked round-bottom flask, and repeatedly heated and degassed under vacuum. The Se precursor solution was rapidly injected into the Cd precursor once it was heated to 300 °C. The reaction mixture was quickly cooled to 50 °C and allowed to anneal overnight. The QD cores were then purified three times using 1-butanol, acetone, and methanol. Finally, the purified QD cores were suspended in toluene.

The SILAR method was then used to add the ZnS shell to the CdSe QD cores.[44] A fraction of the QD cores was purified and dissolved at 100 °C in a mixture of 1-octadecene, oleylamine, trioctyl phosphate (TOP), and dodecylphosphonic acid in a three-neck round-bottom flask. The mixture was degassed under vacuum to remove water and oxygen and then backfilled with nitrogen gas. The solution was then heated to 160 °C under reflux conditions, and a Zn precursor solution (0.05 M zinc formate in oleylamine) was slowly added to the solution using a syringe pump. Subsequently, a sulfur precursor (0.25 M hexamethyldisilathiane in TOP) was slowly added to the solution, also using a syringe pump. The reaction mixture was kept under these conditions for 30 min to allow the formation and annealing of the ZnS monolayer. The temperature was increased to 170 °C, and the process was repeated to add a second and then a third monolayer shell. The temperature was increased by 10 °C for each added monolayer shell. The resulting QDs were capped with trioctylphosphine oxide (TOPO) and suspended in hexanes.

The core and core/shell QDs were purified and resuspended in chloroform to determine the molarity using absorbance measurements and established molar extinction coefficients.[46] The size of the spherical QDs was calculated using absorption and emission data as well and determined to be 1.32 nm (FWHM = 32 nm) for CdSe and 2.26 nm (FWHM = 39 nm) for CdSe/ZnS. Absorption data are graphed in Fig. 1(A) and were collected with a Thermo Scientific Evolution™ 201 UV-Vis spectrophotometer and a PTI QuantaMaster™ 400.

Fabrication of QD–polymer nanocomposites

QD–PMMA polymer composites were fabricated by solution blending. The batch of CdSe cores was used to manufacture the CdSe–PMMA and, after shelling, the CdSe/ZnS–PMMA polymer nanocomposites. For QD–PMMA, this involved mixing 32 mL chloroform (HPLC Grade, EMD Millipore) with 800.7 ± 0.3 mg of poly(methyl methacrylate) (MW = 120 000) (Aldrich) and 8 mL of 1.7 μM QDs suspended in chloroform (Fig. 1(B and C)). This casting solution was then poured into four 20 mL, 1.5 in diameter, aluminum dish molds (Fisher Scientific) and dried overnight in ambient conditions. Circular composites were removed from the molds and soaked in 18 MΩ-cm water for one day, dried in ambient conditions, and then cut with a razor blade into six 0.5 in × 0.25 in samples; see Fig. 1(D and E) for photographs of slide-mounted QD–PMMA nanocomposites. PMMA polymer controls were prepared in a similar fashion with 40 mL of chloroform.

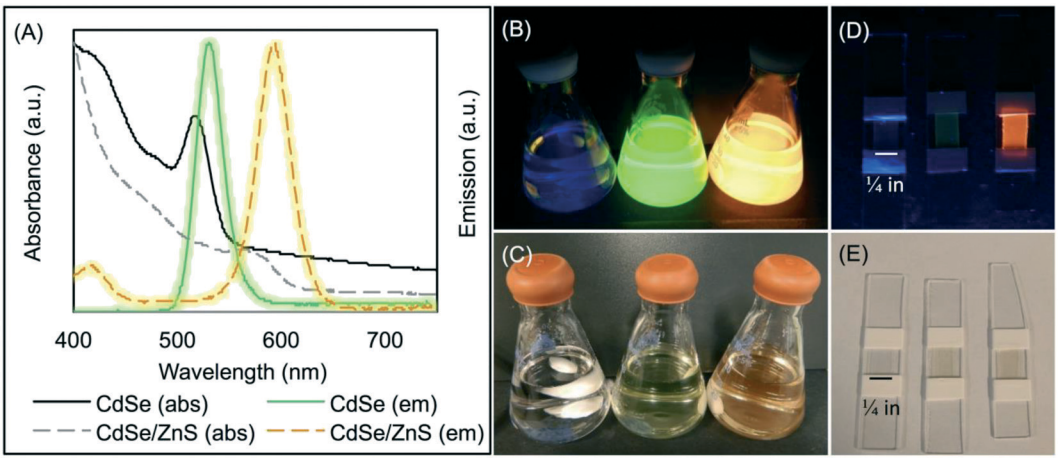

Fig. 1 (A) CdSe nanoparticle (solid lines) and CdSe/ZnS nanoparticle (dashed lines) absorbance and emission in chloroform prior to incorporation into PMMA, where CdSe/ZnS were formed from the CdSe cores indicated here. (B) 365 nm UV and (C) ambient illuminated images of casting solutions in chloroform and (D) 365 nm UV and (E) ambient illuminated images of polymers after solvent evaporation, being cut to size and attached to glass slides with Teflon® tape. The clear PMMA polymer control (left), the green CdSe core control in PMMA (middle) and the orange CdSe/ZnS quantum dots in PMMA (right).

These rectangular samples had an initial mass of: 9.9 ± 0.6 mg (N = 24) for CdSe/ZnS–PMMA, 9.5 ± 0.5 mg (N = 24) for CdSe–PMMA, and 7.4 ± 0.3 mg (N = 24) for PMMA alone. Samples were stored in ambient conditions until use.

Photodegradation of QD–polymer nanocomposites

Samples were secured to a 0.5 in glass slide with 0.25 in PTFE tape (Swagelok®) and placed vertically into 15 mL quartz test tubes, each of which were then filled with 12 mL of 3 μM phosphate buffer, pH 7, in 18 MΩ-cm water (Fig. S1 in the ESI†). The reaction vessel was then capped with a Suba-Seal® septum (Sigma-Aldrich, U.K.) and capped with aluminum foil. The septum was pierced with a 26G needle (BD™) to create a system open to the atmosphere.

Polymer composites were degraded in a 16 lamp Rayonet Photochemical Reactor© with RPR-2537A lamps of 254 nm UVC light (Southern New England Ultraviolet Company, Branford, CT). The photon flux was determined by actinometry to be 2.31×10^{21} quanta s^{-1} m^{-2} with a power density of 1.81 kW m^{-2}, where peak solar radiation is defined as 1 kW m^{-2}.[47] Dark samples were wrapped in aluminum foil and placed in a 30 °C water bath. Samples were irradiated for 210.5 h, 336 h and 504 h, hereafter called 1.25, two and three weeks, respectively. For each irradiation time, system control, PMMA, and QD–PMMA samples were started at the same time. After photolysis, the glass slides with the QD-polymer nanocomposites were removed from the reaction vessels and air-dried for at least 24 h prior to analysis.

The solution in the reaction vessel was partitioned for analysis as follows: 2 mL for pH determination, 7 mL for 0.45 μm syringe filtration (Millipore), nitric acidification (TraceSELECT™, Honeywell Fluka™), and subsequent ICP-MS analysis in an acid-washed 15 mL conical, while the remaining aseptically transferred 3 mL was used for microscopy and bacterial viability studies.

Characterization of QD–polymer nanocomposites

Confocal laser scanning microscopy (CLSM). Solid CdSe/ZnS–PMMA and PMMA samples were analyzed by CLSM before and after photodegradation. In these analyses, 142.86 μm^2 images were acquired at 2048 × 2048 resolution. CLSM images were acquired from the composite surface of the QD–polymer nanocomposites and up to a depth of 5 μm below the surface on a Zeiss LSM 510 META confocal microscope using 488 nm excitation. A 505 nm band pass emission filter was chosen to avoid any UV absorption of degraded PMMA. CLSM images were processed in Zen2009 and LSM image browser (Zeiss) and transformed in ImageJ (NIH). To visualize the QD emission from within the QD–polymer nanocomposites before and after photodegradation, 512 × 512 resolution Z-stack images were constructed up to a depth of 64 μm below the surface.

Photoluminescence (PL). The PL of solid QD–polymer composites before and after exposure to UVC irradiation was recorded on a Photon Technology International system using a Newport RSP-1T solid sample holder. In this apparatus, samples are positioned at a 90° angle between the incident LPS-220B lamp power supply (xenon arc lamp source (USHIO Inc., Japan)) and the 814 photomultiplier detection system. Samples were excited at 400 nm and emission collected from 700–425 nm, 1 nm step size, with a 1 nm excitation slit and 1 nm emission slit. To ensure consistency, PL data was collected with the same slit width, on the same day, and are graphed on the same y-axis.

Attenuated total internal reflection Fourier-transform infrared spectroscopy (ATR-FTIR). Changes to the chemical bonding within QD–polymer composites was determined with a Thermo Fisher Scientific Nicolet iS5 FT-IR Spectrometer equipped with iD5 ATR accessory with a diamond laminate crystal. Data was averaged over 64 scans with a 0.8 cm^{-1} resolution, background subtracted, and baseline corrected. Three random spots on the polymer surface were tested to ensure that similar spectra were recorded.

X-ray photoelectron spectroscopy (XPS). Surface analysis of QD–polymer composites was accomplished using a PHI 5600 XPS system equipped with a Mg Kα X-ray (1253.6 eV) source detected at 0.125 eV step size with a pass energy of 59.7 eV. For XPS analysis, analysis, 0.25 in × 0.25 in sections of polymer sample were secured to sample stubs with double sided copper tape (3M™) while suspension-phase QDs were dropcast onto Si substrates. Calibration of the XPS to the C(1s) peak position of hydrocarbon species at 285.0 eV as well as baseline corrections, peak fitting and determinations of atomic concentrations was carried out with CasaXPS software.

Scanning electron microscopy (SEM). 0.25 in × 0.125 in sections of polymer samples were mounted onto aluminum stubs with double-sided carbon tape (3M™) and sputter coated with platinum to minimize charging (Quorum Technologies Polaron SC7640 Auto/Manual High Resolution Sputter Coater, 12 mA/800 V plasma current, 200 s, East Sussex, UK). Images were obtained at 10 or 20 keV, ~8.0 nm WD on a JEOL 6700F SEM.

Solution characterization after photolysis. The pH of the solutions after reaction was determined with a Thermo Fisher Scientific Accumet®XL20 pH Meter equipped with a 9103BNWP electrode calibrated with pH 4, 7 and 10 buffers (Ricca Chemical) or pH paper. The concentration of Cd ($[Cd]_{ttl}$) released into solution as a result of photodegradation was measured using ICP-MS. This involved triplicate sampling of acidified solutions using a PerkinElmer Elan® DRC II ICP-MS with argon carrier gas and a TraceSELECT™ nitric acid carrier solution. A calibration curve was made for every 20 samples by serial dilutions of 1000 μg L^{-1} standard solutions of Cd, Se, Zn, S, P supplied by NIST traceable standards (Inorganic Ventures) to 1, 5, 10, 20, 50, 100 μg L^{-1} concentrations; where necessary the calibration curves were extended to 170 μg L^{-1} and 240 μg L^{-1}. The released cadmium concentration represents the sum of QDs embedded in polymer fragments, ions, and QDs.

Imaging of aqueous solutions containing photodegraded fragments generated by irradiating PMMA, CdSe–PMMA, and

CdSe/ZnS–PMMA composites were acquired using high S/N ratio, dark-field Cytoviva® hyperspectral imaging (HSI). In these experiments, sample solutions were drop-cast (~3–4 μL) onto a glass slide, which was then sealed with a cover slip and clear nail polish. Slides were examined at 100× magnification with an oil immersion lens under an Olympus BX-41 microscope. Scattering spectra were acquired with a Cytoviva® spectrophotometer and integrated CCD camera in both the visible and near-infrared range (400–1000 nm). Spectral analysis of the HSI spectra was performed by the Environment for Visualization software (ENVI 4.4 version). Spectral libraries of CdSe in chloroform, CdSe/ZnS in chloroform, and degraded PMMA fragments were collected and then used by the SAM to identify QD-containing fragments released during photodegradation (Fig. S2 in the ESI†).[48] To determine if photoemissive fragments were released on a time scale shorter than 1.25 weeks, CdSe/ZnS–PMMA and PMMA fragments, which were released after one day of photodegradation in a separate experiment, were analyzed by CLSM in the Zeiss LSM 510 with the same sample preparation as for HSI.

Bacterial assay. To measure toxicity of species released from QD–PMMA nanocomposite photofragments to *S. oneidensis* MR-1, the bacterial preparation and toxicity analysis using drop plate colony counting were adapted from Feng *et al.*[49] Bacteria were stored at −80 °C until ready for use, where some of the frozen stock was transferred to an agar plate to grow overnight at 30 °C. Then, 15 colonies were transferred to 10 mL of Luria-Bertani (LB) broth (BD™) and grown for four hours at 30 °C with 300 rpm shaking to reach the late-log phase (OD ≈ 0.6–1). The bacteria in LB broth were centrifuged at 750 × *g* for 10 min, and the pellet was resuspended in Dulbecco's phosphate-buffered saline (DPBS) (Corning Inc.), which was kept on a nutating mixer at room temperature for 10 min. The bacteria were again centrifuged at 750 × *g* for 10 min and then resuspended in 4-(2-hydroxyethyl)-1-piperazineethanesulfonic acid (HEPES) buffer (2 mM HEPES and 25 mM NaCl, at pH 7.4, Sigma-Aldrich). The bacterial culture was diluted to an OD = 0.02, which is approximately 2×10^7 colony forming units (CFUs) per mL.

The culture was further diluted to 1×10^4 CFUs per mL, prior to exposure to 5-fold dilute supernatants from QD–PMMA nanocomposite degradation samples, or with Cd^{2+} at various concentrations (1, 5, 10, 50, 100, 200, 500 ppb). 80 μL of bacteria were exposed to 80 μL of the diluted supernatants or Cd^{2+} solutions for 60 min, and then six 10 μL aliquots were dropped onto an agar plate for colony counting evaluation.

The agar plate was first prepared by drying for 30 min in a 30 °C incubator before being irradiated with UV light for 15 min to ensure sterility. After the bacteria-containing drops were fully absorbed into the agar, the plates were incubated overnight (for ~20 h) at 30 °C. The viability after each exposure was reported as a ratio to the dark samples. Where the three material replicates showed consistent Cd release, as revealed by analysis with ICP-MS; data from these colony counting experiments were combined and subjected to two-way ANOVA to check for statistical significance of the photodegraded samples compared to the dark samples.

Results

Materials characterization of QD and QD–polymer nanocomposites prior to irradiation

Core and core/shell QDs were suspended in chloroform due to functionalization with TOPO and were also miscible with PMMA dissolved in chloroform (Fig. 1(B and C)). The resultant solution-blended CdSe/ZnS–PMMA and CdSe–PMMA polymer nanocomposites, fabricated from the same batch of QD cores, emitted orange and green, respectively (Fig. 1(D and E)), consistent with the color of the respective QDs in solution (Fig. 1(A)). In contrast, the control, PMMA, was transparent and colorless. Following polymer composite synthesis, and after several days of drying and slide mounting, the CdSe cores embedded within the CdSe–PMMA were observed by eye to lose emission brightness, which was expected due to oxidation of the cores without the protective

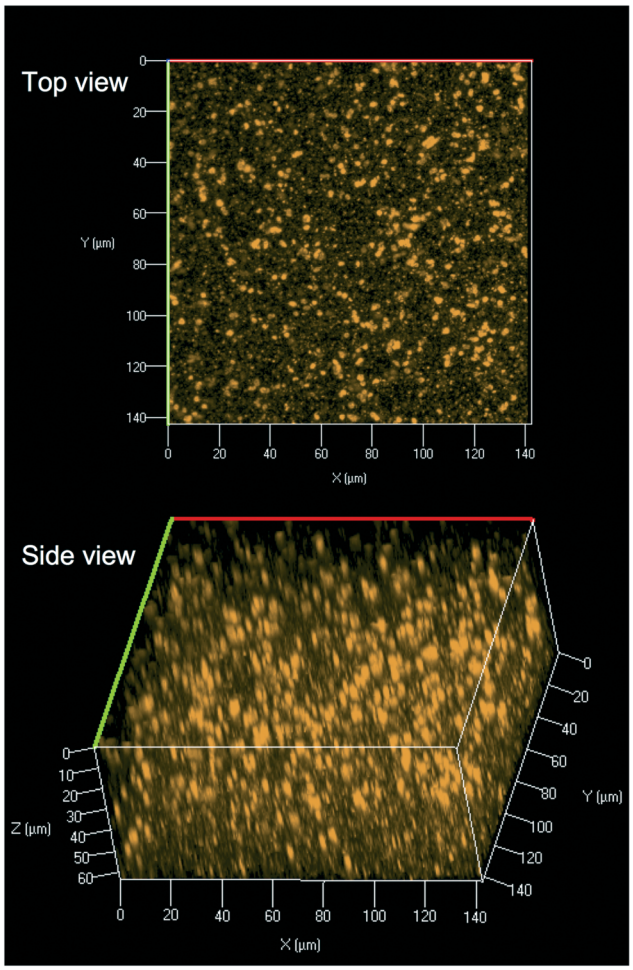

Fig. 2 142.86 μm × 142.86 μm CLSM 64 μm *Z*-stack image of CdSe/ZnS–PMMA polymer nanocomposite obtained with 458 nm excitation. Any emission detected above a 505 nm cut-off filter is shown in orange, which includes the QD λ_{max} = 594 nm.

ZnS passivation layer. The QDs in the CdSe/ZnS–PMMA polymer composites, however, maintained emission for the eight months of this study and continue to emit two years later.

CLSM was used to explore the dispersion of the core/shell QDs within the PMMA matrix. A representative top down and side view image of the dispersion of CdSe/ZnS nanoparticles throughout the polymer matrix within a 142.86 μm × 142.86 μm *Z*-stack of 64 μm is displayed in Fig. 2. The CLSM images were constructed from 80 top down images, acquired with a 0.08 μm step size, stacked on top of each other. Analysis of Fig. 2 revealed the presence of quantum dot agglomerates distributed throughout the polymer matrix. To characterize the size of the QD agglomerates, all emission signals from one high-resolution surface slice of the CdSe/ZnS–PMMA (see Fig. S3 in the ESI†) were classified by the size and spatial distribution of QDs. In ImageJ, this image was globally thresholded and then analyzed with a particle size transform indicating that the 2574 QD agglomerates contained within the 1517 μm^2 area had an average agglomerate size of 0.6 ± 0.6 μm^2.[50]

Polymer thickness was determined with a Leica DMi8A microscope by subtracting the *Z*-height measured when the top of the sample was in focus from the *Z*-height measured when the mounting slide was in focus. In this way, thicknesses of samples used in dark control studies were determined to be 114 ± 15 μm (N = 9) for CdSe/ZnS–PMMA, 104 ± 15 μm (N = 9) for CdSe–PMMA, and 110 ± 20 μm (N = 9) for PMMA samples.

XPS analysis of the CdSe/ZnS nanoparticles and CdSe/ZnS–PMMA nanocomposites revealed the presence of Cd(II) species, evidenced by Cd $3d_{5/2}$ peaks at 404.8 and 404.9 eV, respectively (Fig. S4 in the ESI†). XPS also reveals the presence of S, Se, and Zn before and after solution blending at values close to previous literature assignments for CdSe and ZnS.[51,52] After eight months storage at 5 °C in air in the dark, the CdSe/ZnS QDs had oxidized as determined by the S $2p_{3/2}$ peak at 168.3 eV, consistent with the formation of sulfate species. In contrast, the CdSe/ZnS QDs embedded in PMMA and stored in dark ambient conditions for eight months did not exhibit a shift in the S $2p_{3/2}$ peak, indicating that the PMMA prevented oxygen diffusion (Fig. S4 in the ESI†).[51] In addition to the elements expected for the CdSe/ZnS QDs, and PMMA (oxygen and carbon), residual chlorine from the solvent, chloroform, was detected in the XPS, due to the strong acid–base interaction of acidic chloroform with the basic polymer, PMMA.[53] A small amount of phosphorous was also detected, at a P 2p binding energy of 133–134 eV, in starting materials, dark controls and degraded polymers, likely due to the use of a phosphate buffer or TOPO ligand (Fig. S5–S6 in the ESI†) TOPO has a P 2p binding energy of 133 eV[54] and sodium phosphate and hydrogen phosphate have an average P 2p binding energy of 133.1 ± 0.2 eV (N = 6).[55] Similar results were seen for CdSe–PMMA (Fig. S6 in the ESI†).

ATR-FTIR analysis of PMMA and QD–PMMA polymer nanocomposites revealed that the inclusion of QDs did not change the chemical bonding in the PMMA (Fig. S7–S9 in the ESI†).

Polymer matrix degradation

Visual inspection (Fig. S1†) as well as bright-field, dark-field, and SEM (Fig. 3) images revealed that after three weeks of UVC irradiation, the transparent-orange CdSe/ZnS–PMMA composite became yellowed and opaque with a severely roughened surface topography. The change in visual coloration can be ascribed to the effect of matrix degradation and UV-induced cross-linking that accompanies the photochemical cleavage of the ester groups in PMMA.[35,56] Moreover, SEM images revealed an irregular porous surface was created following photodegradation with UVC.

The mass loss observed from PMMA, CdSe/ZnS–PMMA, and CdSe–PMMA samples after different periods of photolysis is reported in Fig. S10 in the ESI.† Although there is some variability, the mass losses among all three types of samples were within at least three standard deviations of each other, with most of the mass loss occurring between 1.25 and two weeks. Mass loss data indicate neither the rate nor the extent of photodegradation was changed by the presence of QDs in the PMMA.

In XPS analysis of 1.25 week-, two week-, and three week-irradiated CdSe/ZnS–PMMA composites, the presence of carbon and oxygen were revealed, but none of the elements associated with QDs, even after 90 min of Ar^+ sputtering, were apparent. In contrast, Cd, Zn, and S were detected by XPS in the CdSe/ZnS–PMMA composites immersed in water in the dark for 1.25 weeks. Although the Cd signal level was lower than that observed in the as-prepared CdSe/ZnS–PMMA nanocomposites, the Cd signal increased upon Ar^+ sputtering. This initial low Cd signal level was ascribed to the deposition of a thin layer of adventitious carbon on the surface as a result of samples having been immersed in buffered water and subsequently air dried prior to XPS analysis. For samples that had been immersed in water for three weeks, no Cd or Zn signals were observed, presumably due to the presence of a thicker adventitious carbon layer than for the 1.25 week sample. It should be noted that the absence of any detectable Cd release from these dark control samples, see the ICP-MS data, also supports the idea that the decrease in Cd signal observed by XPS is not due to the dissolution of QDs in the near surface region.

The CdSe/ZnS-PMMA, CdSe-PMMA, and PMMA ATR-FTIR spectra were compared to corresponding spectra after 1.25, two, and three weeks of photodegradation (Fig. S7–S9 in the ESI†). A broad –OH stretch appeared at 3500 cm^{-1} for all three genres of composites. Characteristic PMMA vibrational modes, such as the C-H (sp^3, stretch) at 2985 cm^{-1}, were lost. The C═O stretch at 1721 cm^{-1} and C–O stretch at 1236 cm^{-1} lost intensity and broadened.[57] Finally, C–O–C band reduction occurred at 1190 cm^{-1}.[58]

Photoluminescence degradation

In Fig. S11 in the ESI,† the PL spectra acquired from solid CdSe/ZnS-PMMA (orange dashed) is compared to that acquired from solid PMMA (blue dotted), after being immersed

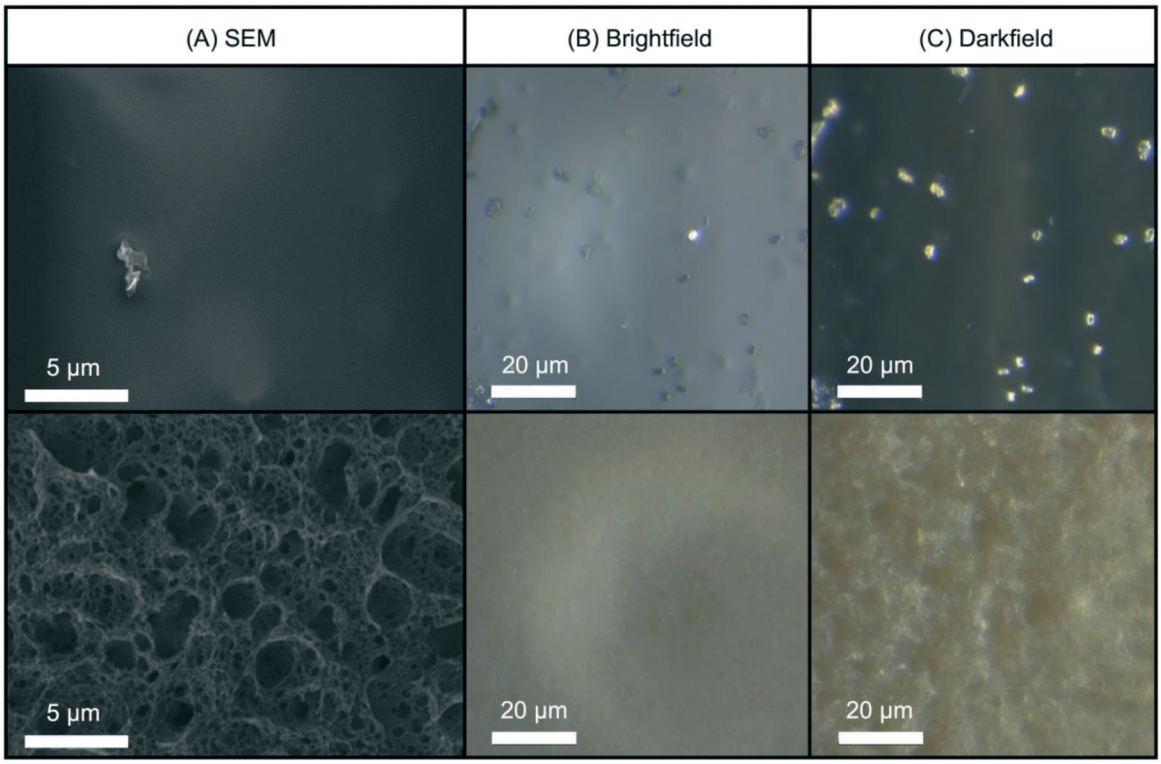

Fig. 3 (A) SEM, (B) bright-field, and (C) dark-field images of the CdSe/ZnS–PMMA nanocomposite surface before (top) and after (bottom) three weeks of UVC irradiation.

in water in the dark for 1.25 weeks. The fluorescence of CdSe/ZnS QDs embedded in PMMA was retained, as evidenced by the emission peak centered at 575 nm λ_{max} ($N = 3$). This represents an ~20 nm blue-shift from the 594 nm λ_{max} peak observed from the CdSe/ZnS QDs when suspended in chloroform (Fig. 1(A)). The 575 nm peak, due to QD emission, is more clearly seen in the difference spectra[59] between the PMMA and CdSe/ZnS-PMMA nanocomposite (black line, Fig. S11 in the ESI†). As expected, no fluorescence was detected in the PL or CLSM for the nanocomposite samples that contained either the weakly fluorescent CdSe QD core controls or the PMMA control.

Following photodegradation, the PL spectra of CdSe-PMMA and CdSe/ZnS-PMMA samples were found to be similar, with a broad peak centered at ~500 nm. The signal of the broad peak increased in intensity as the duration of photodegradation increased, from 1.25-weeks to two-weeks. The presence of this broad feature was also detected in the degraded PMMA samples. Notably, for the photodegraded CdSe/ZnS-PMMA samples, the emission peak at 575 nm no longer appeared, indicating no emissive QDs were left on the surface (Fig. 4(A)).

The three-week irradiated and dark control CdSe/ZnS-PMMA samples were imaged in Lambda mode with the CLSM wavelength-dependent detector, where emission was detected every 10 nm. Two representative CLSM images acquired at 584 nm and 530 nm are shown in Fig. 4; the full 10 image spectrum is provided in Fig. S12 in the ESI.† After three weeks in the dark, the CdSe/ZnS-PMMA sample exhibited discrete features at 584 nm as seen in Fig. 4(B), close to the expected emission λ_{max} = 594 nm and indicative of the presence of embedded QDs. In contrast, no emission was detected at 530 nm. After three weeks of photodegradation, however, there was no evidence of any emission at 584 nm. In contrast, at 530 nm, diffuse emission was now detected in the photodegraded CdSe/ZnS-PMMA and PMMA samples (Fig. 4(A) and (C), respectively) due to fluorescence associated with photodegraded PMMA.

Solution results

Acid. Initially set at pH 7, the solutions exceeded the buffering capacity of the matrix as significant mass loss led to the release of acidic species and CO_2. Consequently, the buffering capacity was found to remain for one day before dropping into an acidic range (see Table S1 in the ESI†).

Cadmium release. Over the three week period, the amount of cadmium released from solution remained stable for both the core control and core/shell composites (Fig. 5). The amount of cadmium released from the CdSe–PMMA nanocomposites after 1.25 weeks was 325 ± 4 μg L^{-1}, which was higher than the 187 ± 16 μg L^{-1} released for CdSe/ZnS–PMMA nanocomposites. This trend was continued to two- and three-weeks with 361 ± 18 μg L^{-1} compared to 209 ± 9 μg L^{-1} and 330 ± 8 μg L^{-1} compared to 194 ± 10 μg L^{-1}, respectively. No cadmium was detected in any of the PMMA, system control, or dark samples.

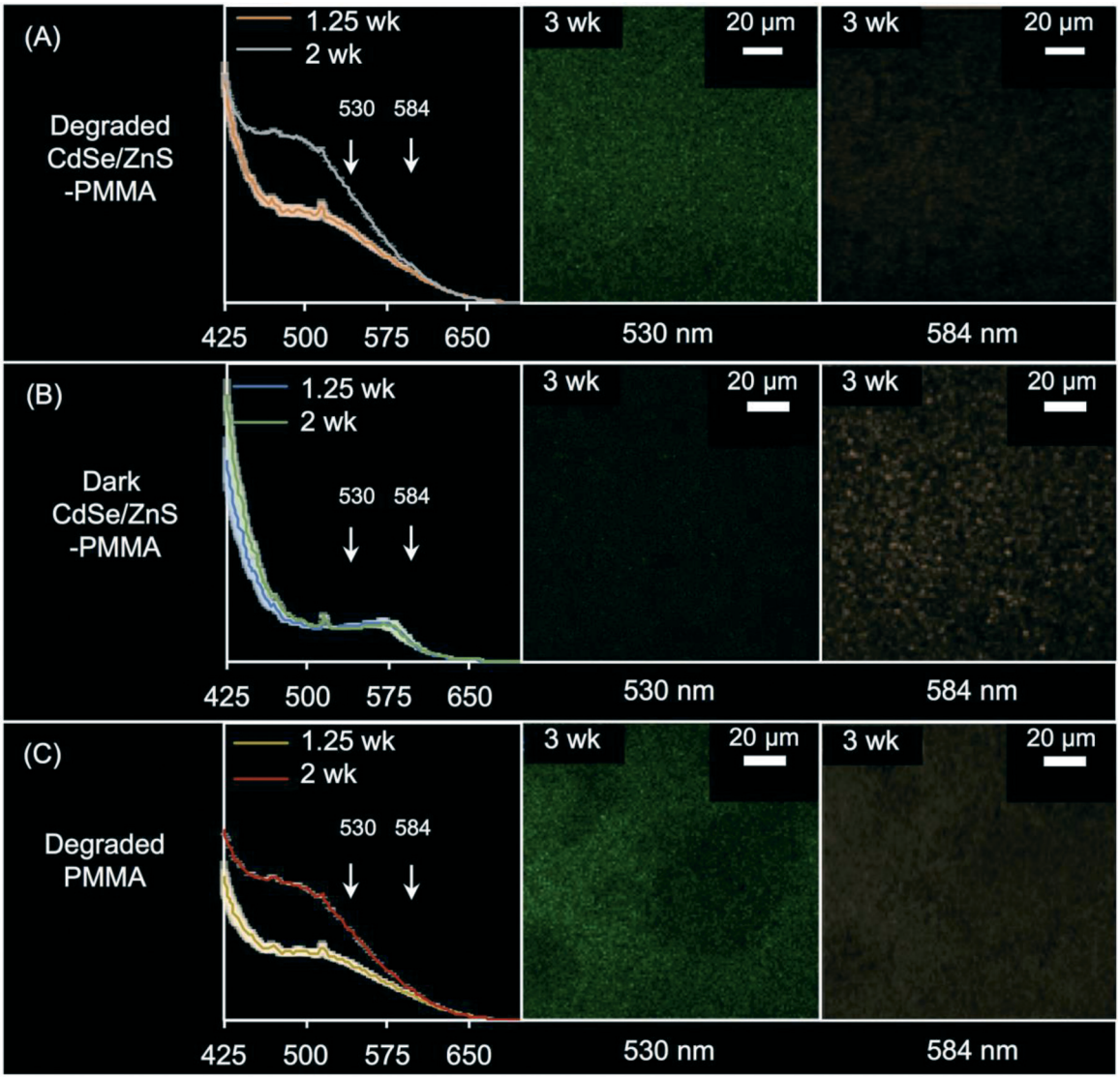

Fig. 4 (Left hand side) Photoluminescence (PL) spectra and (right hand side) CLSM images of solid samples: (A) CdSe/ZnS-PMMA after UVC irradiation, (B) dark CdSe/ZnS-PMMA, and (C) PMMA after UVC irradiation. PL spectra were acquired after 1.25 and two weeks of UVC irradiation ((A) and (C)) or at 30 °C in the dark (B), while CLSM images were acquired after three weeks. The 142.86 μm^2 CLSM images of the three different polymer surfaces were obtained using a 405 nm laser and 10.0% power in lambda detection mode. Other experimental details can be found in the text.

Detection of QD-containing fragments – CLSM. >505 nm emission ascribed to the QDs was detected within released polymer fragments with CLSM after one day of photodegradation. Therefore, some of the cadmium detected in the ICP-MS was from quantum dots embedded in polymer fragments. After one day of photodegradation, see Fig. 6(A–C), emission (labeled orange) was detected from three CdSe/ZnS–PMMA fragments that were 2.7 μm, 4.5 μm, and 6.4 μm in size. No emission was detected in PMMA fragments, see Fig. 6(D), degraded under the same conditions.

Detection of QD-containing fragments – CytoViva®. >505 nm emission could not be detected from nanocomposite fragments beyond one day of photodegradation. Therefore, QDs in fragments were detected with another technique, HSI, as described in the experimental section. A representative image of QDs detected within a degraded PMMA fragment can be found in Fig. 7. After three weeks of degradation, the suspension containing released species from the CdSe/ZnS–PMMA sample was imaged with both dark-field (Fig. 7(A)) and HSI (Fig. 7(B)) microscopy. Degraded polymer fragments were detected as bright spots in the dark-field images (Fig. 7(A)) due to scattered light: the toroidal appearance of the fragments is an artifact of the illumination scheme and the reflective nature of the fragments. Any QDs were located by SAM within the polymer fragments by matching the pixel spectra in the HSI (Fig. 7(B)) to the references in the library yielding a map of CdSe/ZnS in yellow and degraded PMMA in cyan (Fig. 7(C)). To observe detail, the boxed region in Fig. 7(C) was enlarged in Fig. 7(D–F). In contrast, when using the same spectral libraries, no QDs were detected in photofragments

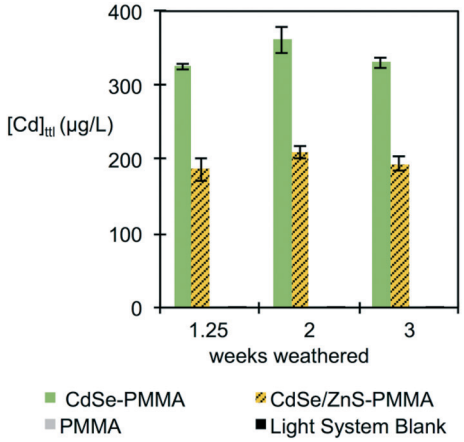

Fig. 5 Total cadmium released from QD–PMMA as detected by ICP-MS for CdSe–PMMA (green), CdSe/ZnS–PMMA (orange), PMMA (grey) and light system blank (black) after 1.25, two and three weeks in the Rayonet© reactor photodegraded with UVC light (N = 3).

generated from pure PMMA (Fig. S13 in the ESI†). When particles were illuminated under the same brightness conditions, CdSe/ZnS QD peaks were strong and sharp while PMMA peaks were broad and of low intensity (as shown in Fig. 7, region of interest (ROI) #1–4). The spectral library filter function was used to validate that there was no spectral overlap between the QD libraries and the PMMA library (Fig. S2 in the ESI†). Subsequently, taking advantage of SAM classification, degraded PMMA photofragments were detected amongst the photofragments created from all three weeks for CdSe/ZnS–PMMA and CdSe–PMMA (Fig. S14–S18 in the ESI†). Many of the detected QDs within these images are co-localized with degraded PMMA signals. Hence, these localized images indicate released QDs can be differentiated from degraded PMMA with HSI using characteristic spectral libraries.

Bacterial data

Using colony counting, the bacterial toxicity of the suspension containing fragments and species generated during the photodegradation of QD–PMMA nanocomposites and PMMA polymers was evaluated. No reduction in viability was observed for the samples that had been degraded for 1.25 weeks (Fig. 8(A)), but after two weeks of degradation, the CdSe–PMMA nanocomposite degradants exhibited toxicity to *S. oneidensis* compared to the dark control (Fig. 8(B)). For samples photodegraded for three weeks, both the degraded CdSe–PMMA nanocomposites and degraded CdSe/ZnS–PMMA nanocomposites, showed significant toxicity to the bacteria (with $p < 0.01$) compared to dark controls (Fig. 8(C)). In ion control experiments, see Fig. 8(D), Cd^{2+} was revealed to be toxic to *S. oneidensis* at concentrations of 200 μg L^{-1} and 500 μg L^{-1}. In contrast, less than 200 μg L^{-1} of Cd^{2+} ion was contained within the 5-fold diluted degradant samples, see ICP-MS data, suggesting viability reduction due to degradants cannot be solely attributed to Cd^{2+} ion. The trend in toxicity of the nanocomposite degradants indicates that as the nanocomposites were subjected to photodegradation for longer time periods, the released fragments were further degraded to more toxic forms.

Discussion

The quality of the QD-polymer nanocomposites was demonstrated by using a combination of microscopy and spectroscopy. A comparison of the starting material data shown in Fig. 1, as well as Fig. 2 and S11 in the ESI,† demonstrate that the optical properties of the CdSe/ZnS QDs are conserved when embedded within the PMMA matrix through solution blending. Visually, this is supported by the observation that both the orange emission and absorption color of the CdSe/ZnS QDs dissolved in chloroform (Fig. 1(B and C)), as well as the emission characteristics of the CdSe/ZnS QDs (Fig. 1(A)), are retained when the QDs are embedded in PMMA (Fig. 1(D and E) and S11). Fig. 1(A) reveals the general retention of QD emission properties. The peak at 572 nm in the CdSe/ZnS–PMMA solid composites (observed in the PL data in Fig. 4(B) and Fig. S11 in the ESI†), however, is blue shifted from the 594 nm emission peak of the CdSe/ZnS QDs in chloroform which might be attributed to solvent effects and sub-nanometer QD surface oxidation during the nanocomposite manufacturing process.[45,59] Emission was rapidly lost from the CdSe QDs embedded in the PMMA, highlighting the importance of the ZnS shell in protecting the CdSe core. Prior to irradiation, the presence of QDs dispersed

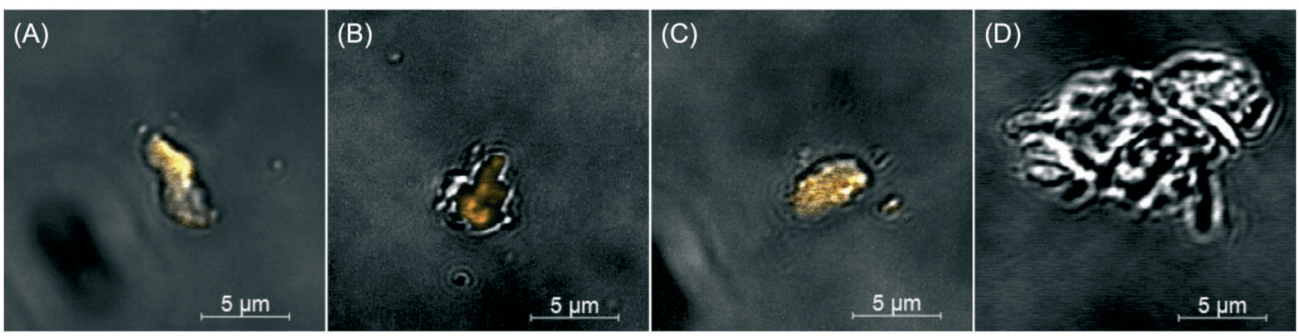

Fig. 6 CLSM images of fragments released from CdSe/ZnS–PMMA (A–C) and PMMA (D) after one day of UVC irradiation, where orange indicates any emission detected above 505 nm.

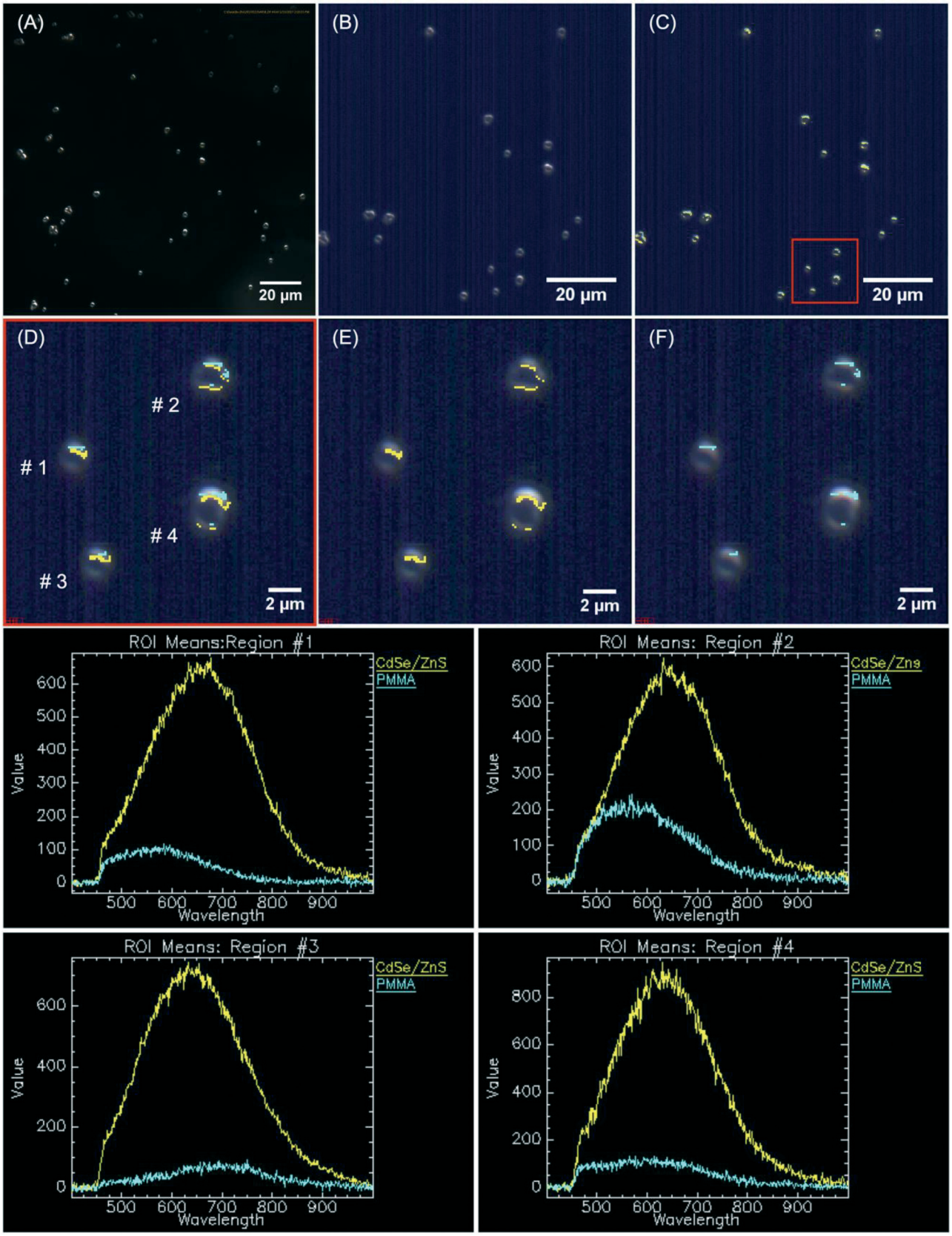

Fig. 7 (A) Dark-field image and (B) hyperspectral image (HSI) of CdSe/ZnS–PMMA fragments released after three weeks of UVC irradiation. (C) The HSI was searched for degraded PMMA signal (teal) and CdSe/ZnS nanoparticle signal (yellow). The red zoomed in box shows (D) the co-localization of the signals, (E) the signal from CdSe/ZnS nanoparticle only and (F) the signal from the degraded PMMA only. The region of interest (ROI) spectral profiles below correspond to the labeled fragments #1, #2, #3 and #4 in (D).

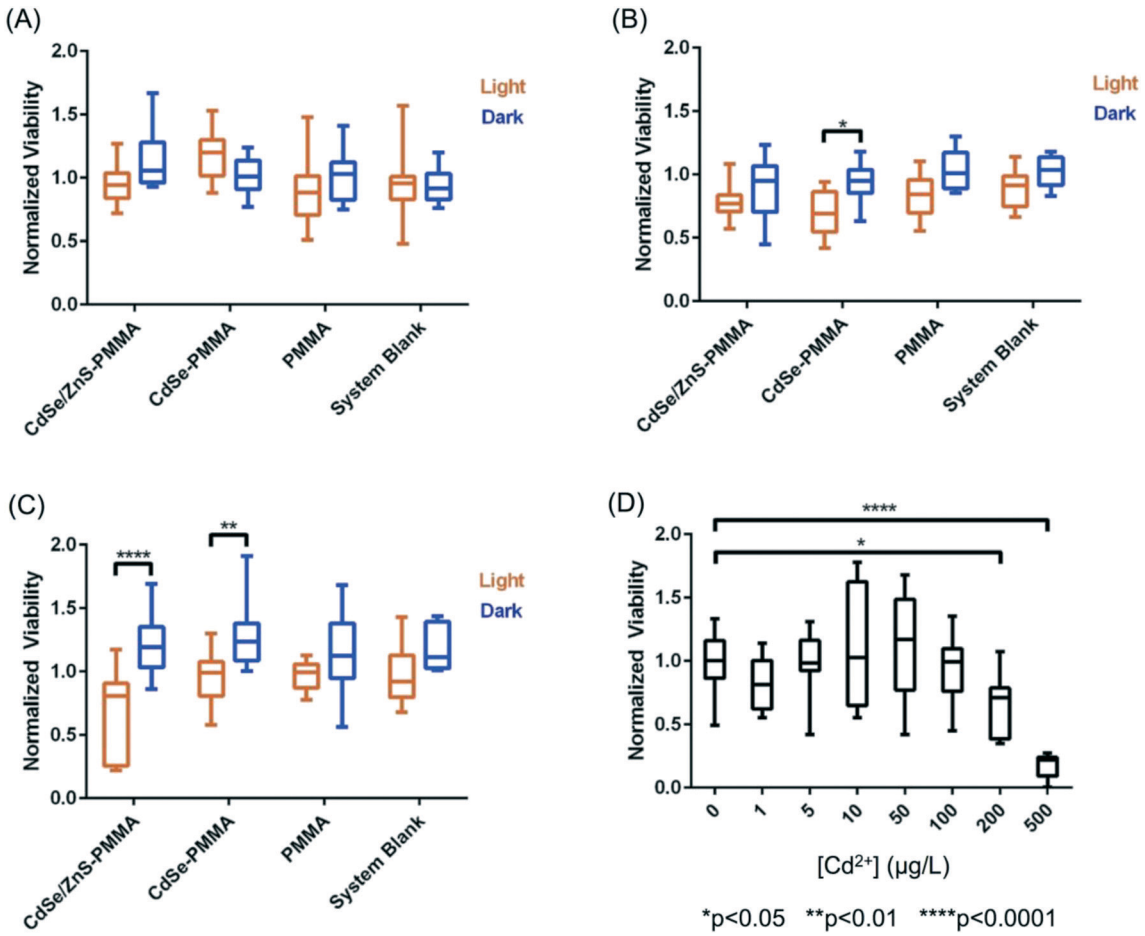

Fig. 8 Toxicity of the degradant products of accelerated QD–PMMA degradation to *S. oneidensis* MR-1 as determined by colony counting using nanocomposites that were degraded for (A) 1.25 weeks, (B) two weeks, and (C) three weeks. (D) The toxicity of Cd^{2+} ions (ion source: $Cd(NO_3)_2 \cdot 4H_2O$) at varying concentrations to the bacteria. The error bars show the range of the data, with the boxes indicating the second and third quartiles of the data.

within the CdSe/ZnS-PMMA matrix is most clearly evidenced by the bright pixelated features detected in the 10 nm detection windows centered around 584 nm and 594 nm in the CLSM images (Fig. 4(B) and Fig. S12 in the ESI†). While a significant degree of QD aggregation was exhibited within the polymer matrix, as shown in the CLSM *Z*-stack (Fig. 2), the agglomerates are reasonably uniformly dispersed within the matrix, with no evidence of any large scale segregation (Fig. S3 in the ESI†). Overall, the CdSe/ZnS–PMMA nanocomposites can be considered a reasonable representation of a QD-polymer nanocomposite found in consumer products, such as LED lighting applications.

Significant polymer matrix photodegradation and production of photofragments was caused by UVC irradiation, demonstrated by the mass loss data (Fig. S10 in the ESI†) as well as the SEM and light microscopy images (Fig. 3). A high degree of photodegradation was also evidenced by the mass loss data with this experimental approach. Micrometer-sized holes in the surface of the material are clearly shown in the SEM image (Fig. 3(D)) which could be a possible source for the 5 μm fragments detected with CLSM (Fig. 6). Furthermore, cleavage of the ester group and subsequent cross-linking of the remaining polymer[35,56] is indicated by a yellowing of PMMA (Fig. 3(E and F) and S1 in the ESI†). In addition to these structural modifications, UVC irradiation led to a loss of spectral features usually seen in the fingerprint region below 1500 cm^{-1} according to the ATR-FTIR data (Fig. S7–S9 in the ESI†). The use of 254 nm UVC light in water as an accelerated weathering technique for simulating matrix degradation is supported by the similarity in the changes in the ATR-FTIR observed in this study and PMMA degraded at 260 nm, 280 nm, and 300 nm in vacuum;[35] specifically the reduction of the C–O–C band intensity at 1190 cm^{-1}. Based on previous studies, matrix degradation can be assumed to occur principally as a consequence of absorption by the carbonyl group in the PMMA, leading to chain scission.[34] The emission properties of the photodegraded PMMA and CdSe/ZnS–PMMA nanocomposites are also transformed according to the PL data in Fig. 4(A), where emission below 575 nm was measurably increased due to photodegradation of the PMMA. A similar increase was not observed in the dark control (Fig. 4(B)). In the CLSM images shown in Fig. 4(A and C), this polymer

degradation was manifested as an increase in diffuse emission at 530 nm. Future research is merited to compare this photodegradation system with past results. Acrylate monomer, CH_3OH, and $HCOOCH_3$ were the photoproducts produced by UVC PMMA film degradation (UHV, 25 °C), as detected by solvent dissolution and GC-MS. Chain scission was determined to be the main photoprocess, with a quantum yield of 0.05 as determined by HPLC.[57] The degraded polymers in the present study were utilized for surface analysis, however, photoproducts and chain scission can be quantified by complete dissolution of the solid polymer into solvent followed by GC-MS and HPLC respectively. The decrease in pH was most likely due to the release of carbon dioxide, which occurs during Norrish type I main chain scission reactions. Due to the resistance of PMMA to acid degradation (<20% hydrochloric, <10% acetic and carbonic acids at 30 °C),[60] any passive acid-based leaching of cadmium ions from the polymer is theorized to be minimal compared to the active release from polymer matrix photodegradation.

Interestingly, although the rate and extent of polymer mass loss was independent of the presence of QDs, see Fig. S10 in the ESI,† the measured $[Cd]_{ttl}$ in the supernatant was consistently higher for the CdSe–PMMA nanocomposites, as compared to the CdSe/ZnS–PMMA composites, although the nominal $[Cd]_{ttl}$ in both types of composites was the same (Fig. 5). This difference may be a consequence of the greater ease with which Cd ions are released from CdSe QDs as compared to CdSe/ZnS QDs, coupled with the likelihood of a greater efficiency for Cd detection by ICP-MS from Cd ions as compared to Cd contained in either intact QDs or in polymer fragments.

In addition to matrix degradation, the bright-field images shown in Fig. S1 in the ESI,† as well as the CLSM images shown in Fig. 4 and S12 in the ESI,† imply the absence of any emissive QDs after the composites are irradiated for 1.25 weeks. This assertion is supported by the similarity in the PL spectra of irradiated CdSe/ZnS–PMMA nanocomposites and irradiated PMMA (compare PL spectra in the left-hand side of Fig. 4(A and C)). In the CLSM data, (compare the right-hand side of Fig. 4(A and C)), the diffuse emission at 530 nm observed in photodegraded CdSe/ZnS–PMMA nanocomposites is observed in photodegraded PMMA, but the initial 594 nm QD emission in non-photodegraded CdSe/ZnS–PMMA is absent after three weeks of photodegradation.

Fragments were released due to active polymer matrix photodegradation, as demonstrated by microscopy (Fig. 6 and 7 and S13–S18 in the ESI†), which occurs in all three sample types: PMMA, CdSe–PMMA, and CdS/ZnS–PMMA. Moreover, for CdSe–PMMA and CdSe/ZnS–PMMA, nanoparticles are contained within released polymer fragments in addition to ions detected in ICP-MS. In contrast, only ions or ions attributed to discrete QDs were detected in previous passive release studies involving QD–polymer composites.[9,21,22] Although the QDs introduced into the PMMA are initially coated with TOPO and insoluble in water, as a result of the polymer degradation process some of these nanoparticles become embedded in polymer fragments which appear to be mobile in aqueous media, and will therefore likely transport in aqueous environments. This assertion is based on our experimental observations that in both the dark-field and Cytoviva microscopes, the QD-containing fragments were mobile.[61]

The species released in passive release studies, Cd ions and discrete QDs,[9,22] have the potential to be toxic to a variety of different organisms. In contrast, this study focused on identifying the nature and toxicity of QD-containing fragments that will be released during active polymer nanocomposite degradation processes such as weathering. During the initial stages of matrix degradation, the release of polymer fragments containing emissive QDs was identified with CLSM (Fig. 6). Although CdSe/ZnS QDs are efficiently photobleached by 1.25, two, and three weeks of UVC photolysis, polymer degradation occurs in parallel, evidenced by the significant observed mass losses (Fig. S10 in the ESI†). Consequently, during the initial stages of polymer photodegradation, some optically-intact QD-containing fragments are released into solution, and it is these fragments that are detected by CLSM in Fig. 6. As the photodegradation process proceeds, however, QDs in the solid substrate polymer matrix, or in solution as released polymer fragments, will become photobleached. Consistent with this argument, QDs embedded in PMMA substrates and fragments were rapidly photobleached.

QD-containing fragments were released into solution intact throughout weeks of accelerated artificial weathering. Individual QDs would not be detected through the methods used, as the diffraction-limited resolution of CLSM is ~200 nm. Cadmium-containing species, <0.45 μm in size, were detected with ICP-MS. More cadmium was released for the CdSe–PMMA than for the CdSe/ZnS–PMMA due to the lack of a protective ZnS passivation shell that exposed the core to oxidation. If the QDs had fully dissolved into their ions, then there would have been no dark-field scattering signature in the HSI. In the present study, CdSe QDs, which had lost their emission by exposure to oxygen,[44,45,62,63] could only be identified through their unique HSI spectral signature (Fig. S16–S18 in the ESI†). This is also true for CdSe/ZnS–PMMA fragments after one day of photodegradation. The success of the HSI microscopy in identifying QD-containing fragments generated from CdSe–PMMA and CdSe/ZnS–PMMA suggests that this technique could be applied to other nanoparticle fragments generated from composite materials. A unique scattering spectrum can be generated by each type of nanoparticle, which can then be used as a fingerprint in the training dataset. In this way, the SAM function of the CytoViva® imaging system could locate either individual particles or agglomerates in complex environments *via* fast optical and spectroscopic identification.[38,39] Specifically, HSI is shown to be capable of discriminating between pixels containing PMMA only and those containing CdSe/ZnS QDs (see Fig. 7) based on relatively small differences in the spectral response of these two materials. An internal consistency check on the viability of this approach is also provided by the absence of any CdSe/ZnS-containing fragments being detected in fragments

generated by the photodegradation of PMMA (Fig. S13†), which is a consequence of the different spectral signatures in the material library (Fig. S2†).

The quantification of the size and concentration of photodegraded water-soluble microplastics is a developing field. This study was focused on the detection of quantum dots within released polymer nanocomposites; however, further research is needed to quantify the concentration of these released fragments. As the concentrations of fragments in released solutions and 10× diluted released solutions were below the detection limit of the DLS and UV-vis, microscopy was utilized to identify released material in the form of microplastics. A review of quantification methods in marine debris studies found 6 of 68 papers utilized a pre-massed 1–1.6 μm filter to capture and mass the >1 μm fragments in marine samples, which would be the best method to quantify the concentration of 5 μm PMMA fragments like those found here.[64]

The viability of *S. oneidensis* was studied when exposed to released photofragments which are a combination of released polymer composite fragment colloids, photobleached QDs, and aqueous species such as cadmium, selenite, zinc, and sulfate ions. In terms of toxicity, cadmium ions are generally considered to be the most important species in quantum dot toxicity with bacteria,[62,65] however, in our studies the viability reduction seen in *S. oneidensis* after exposure to photodegraded nanocomposites occurs in the absence of any change to the $[Cd]_{ttl}$ and therefore is not entirely due to Cd^{2+} ions. Specifically, Fig. 8 shows a statistically significant toxicity of CdSe–PMMA and CdSe/ZnS–PMMA nanocomposites photodegraded for two and three weeks (Fig. 8(B and C)) and three weeks (Fig. 8(C)), respectively. In contrast, no evidence of toxicity towards *S. oneidensis* was shown for the degraded PMMA samples for the duration of the experiments. *S. oneidensis* has been shown to be insensitive to zinc and selenite, the most abundant form of dissolved selenium,[62] at the concentration relevant in this study.[66,67] Hence, the main species responsible for the increased toxicity is postulated to be the released QD-containing fragments. The increase in toxicity of the released fragments as a function of UVC exposure, despite the absence of a change in the $[Cd]_{ttl}$, is interpreted to indicate that weathering changed the toxicity of the QD-containing polymer fragments. As the nanocomposites are continually exposed to UVC light, we speculate the size of the fragments decreased, exposing more QDs to the fragment surface. Uptake of either 1.32 or 2.26 nm QDs or 5 μm QD-containing fragments (see Fig. 6) would, most likely, not occur with *S. oneidensis*, as proven with TEM for similarly-sized gold nanomaterials.[49,68] 4 nm-diameter nanoparticles, however, can associate with the outer bacterial membrane of *S. oneidensis*, as observed by TEM in Buchman *et al.*[68] Similarly, QD-containing polymer fragments could attach to the outer surface of *S. oneidensis*. These smaller fragments, with more QDs at the surface, could be a source for high local concentration of QDs and/or Cd^{2+} at the bacterial membrane as they degraded.

Conclusions

Micron-sized polymer fragments containing nanoparticles, such as QDs, will be released from polymer nanocomposites during active release scenarios like weathering and abrasion. In this study, HSI and CLSM imaging have been shown capable of observing this type of QD release into solution. Identification of these nanoparticle-containing fragments is far more challenging than the detection and quantification of ions. The current study also demonstrates the ability of HSI to detect QD-containing polymer fragments and to distinguish them from polymer-only fragments. Importantly, HSI does not require QDs to exhibit photoluminescence to be detected because their presence can be identified through a unique light scattering spectral signature. The major mechanism of ion and nanoparticle fragment release in this study was through photodegradation of the PMMA matrix, which occurred through chain scission and cross-linking. Although this model polymer nanocomposite was synthesized in a laboratory environment, the conclusions are nevertheless applicable to commercial nanocomposite products. With respect to polymer nanocomposites that have been discarded at product end-of-life, studying the environmental impact of nanoparticles, which have undergone transformation, such as photodegradation, is clearly important in the study of the environmental impact of the pristine nanoparticles used to manufacture the original product. Having identified the release and mobility of QD-containing polymer fragments, it would be useful, in future studies, to determine the fate and transport of QD–polymer fragments in porous media, as well as the stability of QD-containing polymer fragments towards dissolution and fragmentation in various aqueous environments. In the present study, the toxicity of polymer fragments towards the model organism *S. oneidensis* was demonstrated. To obtain a more complete picture of ecotoxicity, it would be valuable to test the toxicity of QD-containing polymer fragments to more metal-sensitive bacteria such as *Acinetobacter baylyi* and *Pseudomonas aeruginosa*.

Conflicts of interest

The authors declare no competing financial interest or conflict of interest.

Acknowledgements

This work was funded by the Center for Sustainable Nanotechnology under the National Science Foundation Center for Chemical Innovation Grant CHE-1503408. J. T. B. acknowledges support by the University of Minnesota Biotechnology Training Grant Program through the National Institutes of Health Grant 5 T32 GM 8347-24. The authors would like to acknowledge the following individuals for consultation and method development: Erin Pryce for CLSM, Bernard Gaskey for SEM and light microscopy, Ronald Lankone for composite fabrication, and Heredeline Ardona for PL. The authors thank the Department of Geographical and Environmental Engineering,

the Integrated Imaging Center, Surface Characterization Facility, and the Tovar Lab at Johns Hopkins University for use of their instrumentation.

References

1 Project on emerging nanotechnologies, *Consumer Products Inventory*, 2013, https://www.nanotechproject.org/cpi, (accessed April 2017).
2 B. T. Branson, M. A. Seif, J. L. Davidson and C. M. Lukehart, Fabrication and macro/nanoscale characterization of aggregated and highly de-aggregated nanodiamond/polyacrylonitrile composite thick films, *J. Mater. Chem.*, 2011, **21**, 18832–18839.
3 Y. Liu and S. Kumar, Polymer/carbon nanotube nano composite fibers: A review, *ACS Appl. Mater. Interfaces*, 2014, **6**, 6069–6087.
4 I. L. Gunsolus and C. L. Haynes, Analytical aspects of nanotoxicology, *Anal. Chem.*, 2016, **88**, 451–479.
5 Y. Yang, Y. Zheng, W. Cao, A. Titov, J. Hyvonen, J. R. Manders, J. Xue, P. H. Holloway and L. Qian, High-efficiency light-emitting devices based on quantum dots with tailored nanostructures, *Nat. Photonics*, 2015, **9**, 259–266.
6 C. W. Tang and S. A. VanSlyke, Organic electroluminescent diodes, *Appl. Phys. Lett.*, 1987, **51**, 913–915.
7 J. M. Pietryga, Y.-S. Park, J. Lim, A. F. Fidler, W. K. Bae, S. Brovelli and V. I. Klimov, Spectroscopic and device aspects of nanocrystal quantum dots, *Chem. Rev.*, 2016, **116**, 10513–10622.
8 S. Liu, W. Liu, W. Ji, J. Yu, W. Zhang, L. Zhang and W. Xie, Top-emitting quantum dots light-emitting devices employing microcontact printing with electricfield-independent emission, *Sci. Rep.*, 2016, **6**, 22530.
9 J. Liu, J. Katahara, G. Li, S. Coe-Sullivan and R. Hurt, Degradation products from consumer nanocomposites: A case study on quantum dot lighting, *Environ. Sci. Technol.*, 2012, **46**, 3220–3227.
10 Y. Shirasaki, G. Supran, M. G. Bawendi and V. Bulović, Emergence of colloidal quantum dot light emitting technologies, *Nat. Photonics*, 2013, **17**, 13–23.
11 Y. Yuan and M. Krüger, Hybrid materials for light conversion applications, *Polymer*, 2012, **4**, 1–19.
12 T. L. Rocha, N. C. Mestre, S. M. T. Sabóia-Morais and M. J. Bebianno, Environmental behaviour and ecotoxicity of quantum dots at various trophic levels: A review, *Environ. Int.*, 2017, **98**, 1–17.
13 V. K. Sharma, T. J. McDonald, M. Sohn, G. A. K. Anquandah, M. Pettine and R. Zboril, Assessment of toxicity of selenium and cadmium selenium quantum dots: A review, *Chemosphere*, 2017, **188**, 403–413.
14 J. L. Pelley, A. S. Daar and M. A. Saner, State of academic knowledge on toxicity and biological fate of quantum dots, *Toxicol. Sci.*, 2009, **112**, 276–296.
15 M. Kondoh, S. Araragi, K. Sato, M. Higashimoto, M. Takiguchi and M. Sato, Cadmium induces apoptosis partly via caspase-9 activation in HL-60 cells, *Toxicology*, 2002, **170**, 111–117.
16 E. Morelli, P. Cioni, M. Posarelli and E. Gabellieri, Chemical stability of CdSe quantum dots in seawater and their effects on a marine microalga, *Aquat. Toxicol.*, 2012, **122–123**, 153–162.
17 E. Yaghini, K. F. Pirker, C. W. M. Kay, A. M. Seifalian and A. J. MacRobert, Quantification of reactive oxygen species generation by photoexcitation of PEGylated quantum dots, *Small*, 2014, **10**, 5106–5115.
18 A. Galeone, G. Vecchio, M. A. Malvindi, V. Brunetti, R. Cingolani and P. P. Pompa, In vivo assessment of CdSe-ZnS quantum dots: coating dependent bioaccumulation and genotoxicity, *Nanoscale*, 2012, **4**, 6401–6407.
19 W.-H. Chan, N.-H. Shiao and P.-Z. Lu, CdSe quantum dots induce apoptosis in human neuroblastoma cells via mitochondrial-dependent pathways and inhibition of survival signals, *Toxicol. Lett.*, 2006, **167**, 191–200.
20 W. Liu, S. Zhang, L. Wang, C. Qu, C. Zhang, L. Hong, L. Yuan, Z. Huang, Z. Wang, S. Liu and G. Jiang, CdSe quantum dot (QD)-induced morphological and functional impairments to liver in mice, *PLoS One*, 2011, **6**, e24406.
21 T. V. Duncan, Release of Engineered Nanomaterials from Polymer Nanocomposites: the Effect of Matrix Degradation, *ACS Appl. Mater. Interfaces*, 2015, **7**, 20–39.
22 K. V. Pillai, P. J. Gray, C.-C. Tien, R. Bleher, L.-P. Sung and T. V. Duncan, Environmental release of core-shell semiconductor nanocrystals from free-standing polymer nanocomposite films, *Environ. Sci.: Nano*, 2016, **3**, 657–669.
23 ISO Standard 877-1:2009, *Plastics – Methods of exposure to solar radiation – Part 1: General guidance*, 2009.
24 B. Nowack, A. Boldrin, A. Caballero, S. F. Hansen, F. Gottschalk, L. Heggelund, M. Hennig, A. Mackevica, H. Maes, J. Navratilova, N. Neubauer, R. Peters, J. Rose, A. Schäffer, L. Scifo, S. v. Leeuwen, F. von der Kammer, W. Wohlleben, A. Wyrwoll and D. Hristozov, Meeting the needs for released nanomaterials required for further testing: The SUN Approach, *Environ. Sci. Technol.*, 2016, **50**, 2747–2753.
25 Y. Pang, S. S. Watson and L.-P. Sung, Surface degradation process affected by heterogeneity in nano-titanium dioxide filled acrylic urethane coatings under accelerated UV exposure, *Polymer*, 2014, **55**, 6594–6603.
26 W. Wohlleben, C. Kingston, J. Carter, E. Sahle-Demessie, S. Vázquez-Campos, B. Acrey, C.-Y. Chen, E. Walton, H. Egenolf, P. Müller and R. Zepp, NanoRelease: Pilot interlaboratory comparison of a weathering protocol applied to resilient and labile polymers with and without embedded carbon nanotubes, *Carbon*, 2017, **113**, 346–360.
27 R. S. Lankone, J. Wang, J. F. Ranville and D. H. Fairbrother, Photodegradation of polymer-CNT nanocomposites: effect of CNT loading and CNT release characteristics, *Environ. Sci.: Nano*, 2017, **4**, 967–982.
28 ASTM Standard G7/G7M-13, *Standard practice for atmospheric environmental exposure testing of nonmetallic materials*, 2013.

29 ASTM Standard G90-10, *Standard practice for performing accelerated outdoor weathering of nonmetallic materials using concentrated natural sunlight*, 2010.
30 A. Heikkilä, S. Kazadzis, O. Meinander, A. Vaskuri, P. Kärhä, V. Mylläri, S. Syrjälä and T. Koskela, UV exposure in artificial and natural weathering: A comparative study, *AIP Conf. Proc.*, 2017, **1810**, 110004.
31 ASTM Standard G155-13, *Standard practice for operating xenon arc light apparatus for exposure of non-metallic materials*, 2013.
32 J. W. Chin, E. Byrd, N. Embree, J. Martin and J. D. Tate, Ultraviolet chambers based on integrating spheres for use in artificial weathering, *J. Coat. Technol.*, 2002, **74**, 39–44.
33 ASTM Standard G113-16, *Standard terminology relating to natural and artificial weathering tests of nonmetallic materials*, 2016.
34 J. Rabek, *Photodegradation of Polymers: Physical Characteristics and Applications*, Springer, 1996.
35 A. Torikai, M. Ohno and K. Fueki, Photodegradation of poly(methyl methacrylate) by monochromatic light: quantum yield, effect of wavelengths, and light intensity, *J. Appl. Polym. Sci.*, 1990, **41**, 1023–1032.
36 M. D. Montaño, J. W. Olesik, A. G. Barber, K. Challis and J. F. Ranville, Single Particle ICP-MS: Advances toward routine analysis of nanomaterials, *Anal. Bioanal. Chem.*, 2016, **408**, 5053–5074.
37 S. Lee, X. Bi, R. B. Reed, J. F. Ranville, P. Herckes and P. Westerhoff, Nanoparticle size detection limits by single particle ICP-MS for 40 elements, *Environ. Sci. Technol.*, 2014, **48**, 10291–10300.
38 G. A. Roth, S. Tahiliani, N. M. Neu-Baker and S. A. Brenner, Hyperspectral microscopy as an analytical tool for nanomaterials, *Wiley Interdiscip. Rev.: Nanomed. Nanobiotechnol.*, 2015, **7**, 565–579.
39 G. A. Roth, M. d. P. Sosa Peña, N. M. Neu-Baker, S. Tahiliani and S. A. Brenner, Identification of metal oxide nanoparticles in histological samples by enhanced darkfield microscopy and hyperspectral mapping, *J. Visualized Exp.*, 2015, **106**, e53317.
40 M. D. P. S. Peña, A. Gottipati, S. Tahiliani, N. M. Neu-Baker, M. D. Frame, A. J. Friedman and S. A. Brenner, Hyperspectral imaging of nanoparticles in biological samples: Simultaneous visualization and elemental identification, *Microsc. Res. Tech.*, 2016, **79**, 349–358.
41 A. R. Badireddy, M. R. Wiesner and J. Liu, Characterization, and abundance of engineered nanoparticles in complex waters by hyperspectral imagery with enhanced darkfield microscopy, *Environ. Sci. Technol.*, 2012, **46**, 10081–10088.
42 H. H. Hau and J. A. Gralnick, Ecology and biotechnology of the genus *Shewanella*, *Annu. Rev. Microbiol.*, 2007, **61**, 237–258.
43 D.-B. Li, Y.-Y. Cheng, C. Wu, W.-W. Li, N. Li, Z.-C. Yang, Z.-H. Tong and H.-Q. Yu, Selenite reduction by *Shewanella oneidensis* MR-1 is mediated by fumarate reductase in periplasm, *Sci. Rep.*, 2014, **4**, 3735.
44 R. Xie, U. Kolb, J. Li, T. Basché and A. Mews, Synthesis and characterization of highly luminescent CdSe–Core CdS/$Zn_{0.5}Cd_{0.5}S$/ZnS multishell nanocrystals, *J. Am. Chem. Soc.*, 2005, **127**, 7480–7488.
45 T. Y. Lyons, D. N. Williams and Z. Rosenzweig, Addition of fluorescence lifetime spectroscopy to the tool kit used to study the formation and degradation of luminescent quantum dots in solution, *Langmuir*, 2017, **33**, 3018–3027.
46 J. Jasieniak, L. Smith, J. van Embden, P. Mulvaney and M. Califano, Re-examination of the size-dependent absorption properties of CdSe quantum dots, *J. Phys. Chem. C*, 2009, **113**, 19468–19474.
47 C. G. Hatchard and C. A. Parker, A new sensitive chemical actinometer - II. Potassium ferrioxalate as a standard chemical actinometer, *Proc. R. Soc. London, Ser. A*, 1956, **235**, 518.
48 B. Stacy, K. Comfort, D. Comfort and S. Hussain, In vitro identification of gold nanorods through hyperspectral imaging, *Plasmonics*, 2013, **8**, 1235–1240.
49 Z. V. Feng, I. L. Gunsolus, T. A. Qiu, K. R. Hurley, L. H. Nyberg, H. Frew, K. P. Johnson, A. M. Vartanian, L. M. Jacob, S. E. Lohse, M. D. Torelli, R. J. Hamers, C. J. Murphy and C. L. Haynes, Impacts of gold nanoparticle charge and ligand type on surface binding and toxicity to Gram-negative and Gram-positive bacteria, *Chem. Sci.*, 2015, **6**, 5186–5196.
50 W. S. Rasband, *ImageJ*, U.S. National Institutes of Health, Bethesda, Maryland, USA, 1997–2016, https://imagej.nih.gov/ij/.
51 E. Agostinelli, C. Battistoni, D. Fiorani, G. Mattogno and M. Nogues, An XPS study of the electronic structure of the $Zn_xCd_{1-x}Cr_2$(X = S, Se) spinel system, *J. Phys. Chem. Solids*, 1989, **50**, 269–272.
52 K. Laajalehto, I. Kartio and P. Nowak, XPS study of clean metal sulfide surfaces, *Appl. Surf. Sci.*, 1994, **81**, 11–15.
53 G. Wypych, in *Handbook of Solvents*, ChemTec Publishing, Oxford, 2nd edn, 2014, pp. 491–497, DOI: 10.1016/B978-1-895198-64-5.50014-3.
54 A. J. Morris-Cohen, M. D. Donakowski, K. E. Knowles and E. A. Weiss, The effect of a common purification procedure on the chemical composition of the surfaces of CdSe quantum dots synthesized with trioctylphosphine oxide, *J. Phys. Chem. C*, 2010, **114**, 897–906.
55 *NIST X-ray Photoelectron Spectroscopy Database, NIST Standard Reference Database Number 20*, National Institute of Standards and Technology, Gaithersburg, MD, 2000, DOI: 10.18434/T4T88K, (accessed August 2016).
56 J. P. Allison, Photodegradation of poly(methyl methacrylate), *J. Polym. Sci., Part A-1: Polym. Chem.*, 1966, **4**, 1209–1221.
57 A. Gupta, R. Liang, F. D. Tsay and J. Moacanin, Characterization of a dissociative excited state in the solid state: Photochemistry of poly(methyl methacrylate). Photochemical processes in polymeric systems. 5, *Macromolecules*, 1980, **13**, 1696–1700.
58 G. Duan, C. Zhang, A. Li, X. Yang, L. Lu and X. Wang, Preparation and characterization of mesoporous zirconia made by using a poly (methyl methacrylate) template, *Nanoscale Res. Lett.*, 2008, **3**, 118.

59 J. R. Lakowicz, *Principles of Fluorescence Spectroscopy*, Springer, New York, NY, 3rd edn, 2006.
60 *Corrosion data survey – Nonmetals Section*, ed. N. E. Hamner, National Association of Corrosion Engineers, Houston, 5th edn, 1975, pp. 3, 184, 404.
61 M. A. Bevan and S. L. Eichmann, Optical microscopy measurements of kT-scale colloidal interactions, *Curr. Opin. Colloid Interface Sci.*, 2011, **16**, 149–157.
62 S. Mahendra, H. Zhu, V. L. Colvin and P. J. Alvarez, Quantum dot weathering results in microbial toxicity, *Environ. Sci. Technol.*, 2008, **42**, 9424–9430.
63 A. M. Derfus, W. C. W. Chan and S. N. Bhatia, Probing the cytotoxicity of semiconductor quantum dots, *Nano Lett.*, 2004, **4**, 11–18.
64 V. Hidalgo-Ruz, L. Gutow, R. C. Thompson and M. Thiel, Microplastics in the marine environment: A review of the methods used for identification and quantification, *Environ. Sci. Technol.*, 2012, **46**, 3060–3075.
65 J. H. Priester, P. K. Stoimenov, R. E. Mielke, S. M. Webb, C. Ehrhardt, J. P. Zhang, G. D. Stucky and P. A. Holden, Effects of soluble cadmium salts versus CdSe quantum dots on the growth of planktonic Pseudomonas aeruginosa, *Environ. Sci. Technol.*, 2009, **43**, 2589–2594.
66 A. C. M. Toes, J. S. Geelhoed, J. G. Kuenen and G. Muyzer, Characterization of heavy metal resistance of metal reducing *Shewanella* isolates from marine sediments, *Geomicrobiol. J.*, 2008, **25**, 304–314.
67 A. Klonowska, T. Heulin and A. Vermeglio, Selenite and tellurite reduction by *Shewanella oneidensis*, *Appl. Environ. Microbiol.*, 2005, **71**, 5607–5609.
68 J. T. Buchman, A. Rahnamoun, K. M. Landy, X. Zhang, A. M. Vartanian, L. M. Jacob, C. J. Murphy, R. Hernandez and C. L. Haynes, Using an environmentally-relevant panel of Gram-negative bacteria to assess the toxicity of polyallylamine hydrochloride-wrapped gold nanoparticles, *Environ. Sci.: Nano*, 2018, **5**, 279–288.

